Kinematics-free angular momentum trajectories. II. Yukawa-potential numerical examples

Robert A. Leacock and Russell L. Martin
Ames Laboratory, United States Department of Energy and Department of Physics, Iowa State University, Ames, Iowa 50011
(Received 19 March 1979)

The kinematics-free angular momentum trajectory, called the γ trajectory, is illustrated numerically in nonrelativistic potential scattering using Yukawa and exponential potentials of various strengths. The γ trajectory, in contrast to the α (Regge) trajectory, is free of elastic kinematics and so is real for all energies above threshold and real for certain energies below threshold. Resonances are caused when the γ trajectory passes *through* the resonance angular momentum at the resonance energy, and bound states are caused when the γ trajectory passes *near* the bound-state angular momentum at the bound-state energy. Numerical illustrations of the following γ trajectory characteristics are given: the reality of γ, bound-state and resonance production, threshold and high-energy behavior, and collisions of trajectories below threshold. In addition, general properties of γ trajectories in the context of potential scattering are discussed.

I. INTRODUCTION

In a previous investigation[1] an angular momentum trajectory, called the γ trajectory, was introduced and used to analyze selected experimental pion-nucleon, partial-wave, elastic scattering amplitudes. As is well known, the Regge (or α) trajectory is defined as the zero of the inverse S matrix and is real below threshold (bound-state region) and complex above threshold (resonance region). Also well known is that the α trajectory causes bound states or resonances by passing through or near the state angular momentum at the state energy, respectively. In contrast, the γ trajectory is defined as the zero of a function Y which is that part of the partial-wave amplitude denominator which does not contain the elastic kinematics. Because of its definition the γ trajectory is real for all energies above threshold and real for certain energies below threshold, and is an analytic function of the energy at threshold. In addition, the γ trajectory causes bound states or resonances by passing near or through the state angular momentum at the state energy, respectively. This bound-state/resonance behavior of the γ trajectory is the complement of that of the α trajectory recalled above. In general, the γ and α trajectories appear to be complements of one another.[1]

The purpose of the present paper is to provide specific numerical illustrations of the γ trajectory in nonrelativistic potential scattering using Yukawa potentials of five different strengths and an exponential potential. The illustrations provide concrete examples of all of the basic γ-trajectory properties stated in TH, and in addition furnish an opportunity to compare γ and α trajectories for the same potentials, since numerical examples of the α trajectories have been calculated previously for the Yukawa potentials.[2] In addition to the numerical examples, some discussion of the general properties of γ trajectories in the context of potential scattering is presented; in particular, two proofs that γ is real above threshold are given.

In Sec. II the numerical method used to calculate the γ trajectories is given, and the relation of the γ trajectories to the properties of the scattering phase shift δ is discussed. In addition, the energy regions where γ is real are examined. In Sec. III are presented γ trajectories calculated for attractive Yukawa potentials of various strengths and γ trajectories for an exponential potential. The numerical γ trajectories are used as a basis for the discussion of the general properties of γ trajectories. In IV a summary of γ-trajectory properties and conclusions are given.

II. COMPUTATIONAL METHOD; PROPERTIES OF γ

A. Definition of γ; potentials

As discussed in TH, the partial-wave elastic scattering amplitude of two spinless particles,

$$A(E,l)=\{\exp[2i\delta(E,l)]-1\}/2ik\,,$$

may be rewritten as

$$A(E,l)=E^l\cos\pi l/[Y(E,l)+(-E)^{l+1/2}]\,,$$

where $Y(E,l)$ is a meromorphic function of E and l which contains no elastic cut, i.e., no right-hand cut in the energy plane from threshold ($E=0$) to the first inelastic threshold ($E=E_{\rm inel}$). Here E, the energy, is related to k by $E=k^2$, l is the angular momentum index, and δ is the scattering phase shift; this notation differs slightly from that of TH. The relationship between $Y(E,l)$ and the scattering phase shift $\delta(E,l)$, which is useful

for our purpose, is

$$Y(E,l) = E^{l+1/2}\{[\cos\pi l][\cot\delta(E,l)] + \sin\pi l\}\,. \quad (1)$$

The Regge trajectory $\alpha(E)$ is defined as a zero of the denominator of the partial-wave amplitude:

$$Y(E, \alpha(E)) + (-E)^{\alpha(E)+1/2} = 0\,, \quad (2)$$

while the $\gamma(E)$ trajectory is defined as a zero of $Y(E,l)$:

$$Y(E, \gamma(E)) = 0\,. \quad (3)$$

From Eqs. (1) and (3) one obtains a direct relationship between the γ trajectory and the phase shift δ:

$$\gamma(E) - (n+\tfrac{1}{2}) = \delta(E, \gamma(E))/\pi \quad (4)$$

where n is an integer. Equation (4) can be used to obtain $\gamma(E)$ provided $\delta(E,l)$ is known.

Before discussing our numerical method for the computation of $\gamma(E)$, we observe that there is a question as to whether the γ trajectory can pass through half-integer[3] points of angular momentum. For l = half-integer, Eq. (1) appears to yield $Y = (\sin\pi l)E^{l+1/2}$ which, in general, is not zero and so is inconsistent with the definition (3). However, if at the same moment that l is a half-integer, the phase shift is an integral multiple of π, then one has in (1) a zero times an infinite quantity and the value of Y will depend upon the exact way l and δ "pass through" the half-integer angular momentum value. This is precisely what happens with the γ trajectory as can be seen in (4) where γ is a half-integer when δ/π is an integer. Thus, the γ trajectory can pass through half-integer angular momentum values. (For further discussion of related limits see Ref. 4.)

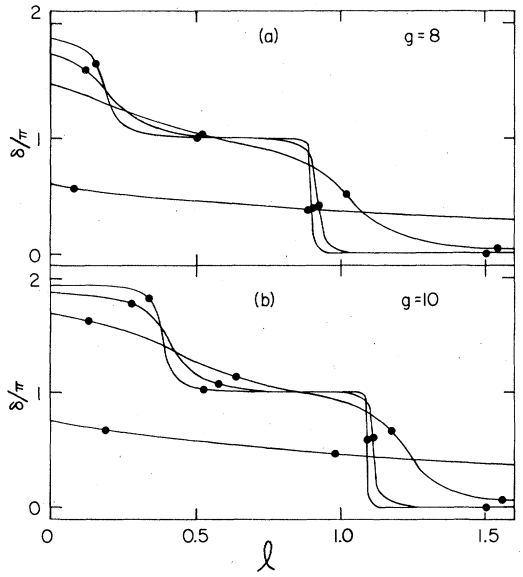

FIG. 1. (a) and (b) The phase shift $\delta(E,l)$ as a function of angular momentum l for fixed, real energy $E > 0$ for the Yukawa potentials $V(r) = -ge^{-r}/r$ with $g = 8$, 10. The energies for the four δ curves shown are, starting from the top curve at $l = 0$: $E = 0.01$, 0.04, 0.25, and 25, respectively. The solid dots on the δ curves are the solutions to Eq. (4), i.e., they mark the intersection of $\delta(E,l)$ and the lines $l - (n+\frac{1}{2})$. These dots give the allowed values of the trajectories $\gamma(E)$ for the given E values. (a) For the case $g = 8$. These δ curves show two $l = 0$ bound states and one $l = 1$ resonance. (b) For the case $g = 10$. These δ curves show two $l = 0$ and one $l = 1$ bound states (see text).

To illustrate the γ trajectory in the context of nonrelativistic potential scattering, we use the attractive Yukawa potential $V(r) = -ge^{-r}/r$ with strengths $g = 8$, 10, and 17, plus, for special purposes, $g = 8.6$ and 9.6. Besides the usual reasons for considering the Yukawa potential, the major advantage for our purposes is that a direct comparison of the γ trajectories for these potentials can be made with α trajectories for the same potentials as previously calculated.[2] In addition to the computations with Yukawa potentials, selected γ trajectories are calculated for the very strong, long-range exponential potential $V(r) = -43e^{-(r/2.5)}$ in order to show specific properties of the γ trajectory which do not arise so easily numerically with the Yukawa potential.

B. Computation of γ: $E > 0$

Our method for the numerical calculation of γ trajectories uses Eq. (4) which directly connects γ with the scattering phase shift δ. (The computation of the phase shift is discussed in Appendix A.) In the above-threshold ($E > 0$) region the phase shift is real for E and l real and from (4), as will be shown, γ is real. The properties of γ follow so closely from those of δ that we first mention briefly the relevant properties of δ that determine the character of γ, in particular those features which indicate bound states and resonances. In Fig. 1 is shown the phase shift (divided by π) as a function of l for the fixed values of the energy $E = 0.01$, 0.04, 0.25, and 25 for Yukawa potentials with strengths 8 and 10. The shoulders and plateaus are a manifestation of Levinson's theorem; as the energy goes to zero from above, the shoulders become very steep and the plateaus have a height which is an integral number, the number giving the number of bound states of that angular momentum. Thus, e.g., from Fig. 1 one sees that the strength 8 Yukawa potential has two $l = 0$ bound states, while the strength 10 potential has two $l = 0$ bound states and one $l = 1$ bound state. In addition, inspection of Fig. 1(a) shows that the

strength-8 potential has an $l=1$ resonance, since the phase shift rises from zero through $\pi/2$ as the energy increases from zero to 0.25 (e.g.). This resonance becomes the $l=1$ bound state of Fig. 1(b) when the potential strength is increased from 8 to 10. We will see in Sec. III how these bound states and resonances manifest themselves in the γ trajectory. Another property of $\delta(E,l)$ that can be seen in Fig. 1, and which directly affects $\gamma(E)$, is that δ vanishes as either $E\to+\infty$ or $l\to+\infty$, as is expected, of course, on physical grounds.

To find $\gamma(E)$ for $E>0$ using graphs such as Fig. 1, we plot both sides of Eq. (4) as a function of l for fixed E, and look for the points of intersection. That is, $l-(n+\frac{1}{2})$ and $\delta(E,l)/\pi$ are plotted versus l, and the points of intersection give the allowed values of $l=\gamma(E)$. This is shown in Fig. 1 where the dark dots on the $\delta(E,l)/\pi$ curves mark the intersections of $\delta(E,l)/\pi$ and $l-(n+\frac{1}{2})$. [The sloping lines $l-(n+\frac{1}{2})$ are not shown.] Thus, the dots of Fig. 1 give the $\gamma(E)$ values for the energies shown. For example, in Fig. 1(a) we see that one γ trajectory has on it the points: $\gamma=0.90$ for $E=0.01$, $\gamma=0.93$ for $E=0.04$, $\gamma=1.02$ for $E=0.25$, and $\gamma=0.89$ for $E=25$. In this manner the trajectories $\gamma(E)$ can be traced out for $E>0$ once $\delta(E,l)$ is calculated. This graphic method of finding $\gamma(E)$ has the advantage of visually connecting the properties of $\gamma(E)$ with those of $\delta(E,l)$; in particular, it is possible to see clearly how resonances are connected with γ.

C. Reality of γ for $E>0$

Inspection of Fig. 1 shows that Yukawa γ trajectories for $E>0$ found by the graphical method outlined in the previous section are real. The questions thus arises: Are all γ trajectories real for $E>0$? The answer to this question is yes, as may be seen by examination of Eq. (4) keeping in mind graphs like Fig. 1. In the set of straight lines, $l-(n+\frac{1}{2})$, each line has a positive slope of unity. In general, the curve $\delta(E,l)/\pi$ is a decreasing function of l and so will cross each line $l-(n+\frac{1}{2})$ only once, thus resulting in a set of unique, "noncolliding" γ trajectories. However, there are two situations which must be examined more carefully. First, $\partial\delta(E,l)/\partial l>-\infty$ for $E>0$ so that two different $l-(n+\frac{1}{2})$ lines cannot intersect $\delta(E,l)/\pi$ at the same l value. Thus, $\delta(E,l)/\pi$ cannot fall rapidly enough to cause two different γ trajectories to "collide." (The only exception to this statement is in the limit $E\to 0$ through positive E values.) A second, possible source of trouble arises if the slope of $\delta(E,l)/\pi$ exceeds unity. In this case $\delta(E,l)/\pi$ could cross a given $l-(n+\frac{1}{2})$ line on the way up and then later, at a higher l, cross the same $l-(n+\frac{1}{2})$ line on the way down. This would result in two γ trajectories from the same $l-(n+\frac{1}{2})$ line. As the energy is increased, and $\delta(E,l)/\pi$ falls, these two trajectories would "collide" and become complex. This possibility of collision is excluded, however, because of the general potential-scattering result bounding the rate of increase of the phase shift[5]: $\partial\delta/\partial l<\pi/2$. Thus, $\delta(E,l)/\pi$ cannot rise so rapidly that two different γ trajectories can collide. In summary, for a given potential, there is a set of real, noncolliding, γ trajectories for energies above threshold. This proof is not valid for energies below threshold, since there the bounds on $\delta(E,l)$ do not exist.

Another proof of the reality of $\gamma(E)$ for $E>0$ based on the radial Schrödinger equation is given in Appendix B.

D. Computation of γ: $E<0$

In the below-threshold ($E<0$), bound-state, region the scattering phase shift is complex, and

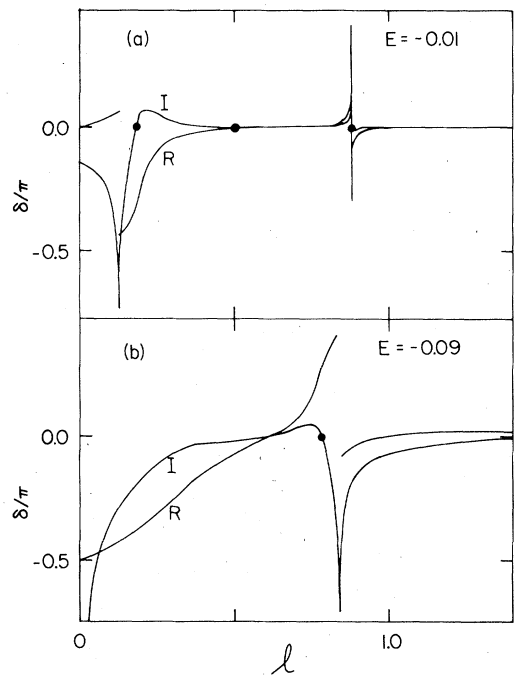

FIG. 2. (a) and (b) The real (R) and imaginary (I) parts of the phase shift $\delta(E,l)$ as a function of angular momentum l for fixed, real energy $E<0$ for the Yukawa potential $V(r)=-ge^{-r}/r$ with $g=8$. The sharp, downward spikes in the imaginary part of δ are bound states (see text). The solid dots on the imaginary part of δ mark the solutions of Eqs. (4) and (5). These dots give the allowed values of the trajectories $\gamma(E)$ for the given E values. The reason that there are three γ solutions in (a) and only one γ solution in (b) is because the two lower γ solutions in (a) have collided and become complex as the energy is decreased from $E=-0.01$ (a) to $E=-0.09$ (b) (see text).

while we still use Eq. (4) to compute $\gamma(E)$, our method differs slightly from the $E>0$, graphic method. In Fig. 2 is shown the phase shift $\delta(E,l)$ (divided by π) as a function of l for $E=-0.01$ and -0.09 for the attractive Yukawa potential of strength $g=8$. The signature of a bound state is that the real part of δ falls abruptly through $\pi/2$, while the imaginary part goes to $-\infty$. Several bound states are seen in the figure; these bound states are unphysical in the sense that a physical bound state must have $l=0,1,2,\ldots$. Properties of the bound states evident from Fig. 2 include (1) the bound states are sharper and narrower in l for energies nearer threshold, i.e., e.g., the $E=-0.01$ bound states are sharper in l than the $E=-0.09$ bound states; (2) the bound states move in l as the energy is changed; (3) there is a correspondence between the shoulders in δ for $E>0$ and the bound states for $E<0$ as can be seen by comparing Fig. 1(a) for $E=0.01$ and Fig. 2(a) for $E=-0.01$. For example, the shoulder at $l=0.90$ for $E=0.01$ "becomes" the "bound state" at $l=0.88$ for $E=-0.01$.

Our method of calculating $\gamma(E)$ for $E<0$ is to use again Eq. (4). We expect, since $\gamma(E)$ is a zero of the real analytic function Y, that $\gamma(E)$ is real for $E<0$ just as it is for $E>0$. (Exceptions to this statement of reality are discussed below.) Assuming for the moment that $\gamma(E)$ is real, we have from (4), since δ is now complex

$$\gamma(E)-(n+\tfrac{1}{2})=\delta_R(E,\gamma(E))/\pi\,,$$
$$0=\delta_I(E,\gamma(E))\,, \tag{5}$$

where R (I) means real (imaginary) part, and where $\gamma(E)$ is understood to be real. Both of Eqs. (5) must be satisfied if $\gamma(E)$ is to be a zero of $Y(E,l)$ and real for $E<0$. Examples of $\gamma(E)$ which satisfy Eqs. (5) are indicated in Fig. 2 by dark dots on the $\delta_I(E,l)/\pi$ curves. For example, there is a solution to (5) in Fig. 2(a): $\gamma=0.88$ for $E=-0.01$. In Fig. 2(b) this solution has moved to $\gamma=0.79$ for $E=-0.09$. [These points are part of the below-threshold continuation of the γ trajectory represented by the four dots near $l=0.9$ to 1.0 in Fig. 1(a) for $E>0$.] Thus, for $E<0$, our method of finding the $\gamma(E)$ is to make a series of figures like Figs. 2(a) and 2(b), and to locate the solutions to (5) on these figures. The $\gamma(E)$ found in this way can then be connected to those $\gamma(E)$ found for $E>0$ by the method of Sec. IIB to give the complete γ trajectories.

The exception to the use of Eqs. (5) for $E<0$ is when γ trajectories collide and become complex. In this case (4) still holds and can be used to find $\gamma(E)$, but now both γ and δ are complex. Examples of such complex γ are shown and discussed in Sec. III.

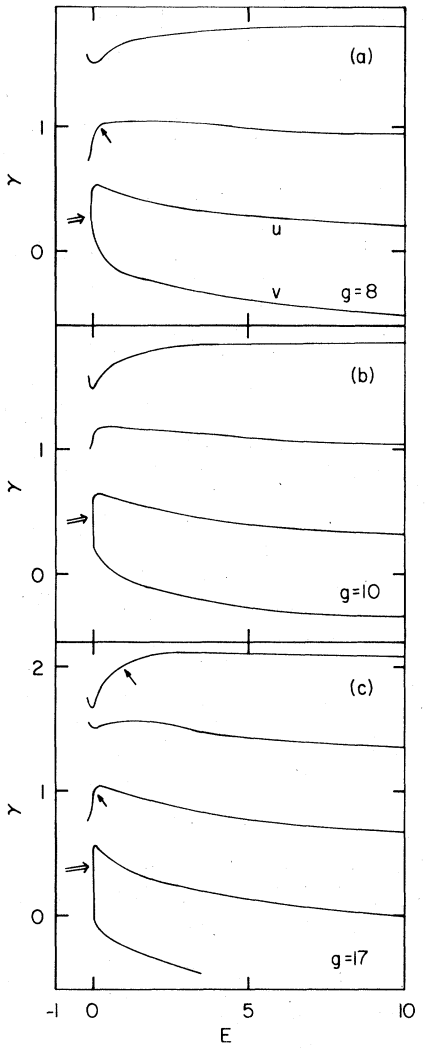

FIG. 3. (a), (b), and (c) γ trajectories for the Yukawa potentials $V(r)=-ge^{-r}/r$ with $g=8$, 10, and 17. The single arrows mark the points where the $\gamma(E)$ cause resonances. The double arrows mark the locations of collisions of two γ trajectories; at these points the colliding trajectories become complex. (a) For $g=8$. Note the $l=1$ resonance at $E=0.19$ (single arrow) caused by the second γ trajectory (see text). The two lowest trajectories (u and v) collide at $\gamma=0.37$, $E=-0.06$ (double arrow) and bounce off into the complex l plane (see text and Figs. 4 and 5). (b) For $g=10$. The second γ trajectory no longer causes a resonance as in the $g=8$ case, but instead now causes a bound state (see text). The lowest two trajectories collide (double arrow). (c) For $g=17$. Note the $l=2$, $E=1.0$ and $l=1$, $E=0.07$ resonances caused by the first and a third γ trajectories, respectively (single arrows). The lowest two trajectories collide (double arrow).

III. γ TRAJECTORIES

A. Yukawa potential: $g=8$

In Fig. 3(a) γ trajectories are shown for the attractive Yukawa potential of strength 8. Details of these $\gamma(E)$ around threshold are shown separately in Fig. 4. In the following discussion we label the individual γ trajectories by their value at threshold $E=0$; e.g., the second (from the top) γ trajectory is called the $\gamma(E=0)=\gamma(0)=0.89$ trajectory. As mentioned in the previous section this potential has two $l=0$ bound states (at $E\simeq-9$ and $=-0.11$), and one $l=1$ resonance (at $E=0.19$). The $l=0$ bound state ($E\simeq-9$) and the $l=1$ resonance are on the leading Regge trajectory, while the other $l=0$ bound state is on a lower α trajectory.[6]

Before discussing the individual γ trajectories we make some general observations. Figures 3(a) and 4 show four γ trajectories with threshold values: $\gamma(0)=1.5$, 0.89, 0.5, and 0.17. The origin of these $\gamma(E)$ in the phase shift $\delta(E,l)$ can be seen in Figs. 1(a) and 2, where it can be noted that the $\gamma(0)=1.5$ and 0.5 trajectories start on the plateaus of δ, while the $\gamma(0)=0.89$ and 0.17 trajectories start on the shoulders of δ. In addition to the γ trajectories shown in Fig. 3(a) and 4, there are higher-lying γ trajectories beginning at $l=\frac{5}{2}$, $\frac{7}{2}, \frac{9}{2}, \ldots$; these trajectories are very similar in character to the $\gamma(0)=1.5$ trajectory which we discuss next. Comparison of the γ trajectories of Fig. 3(a) with the corresponding α trajectory of Fig. 1 of Ref. 2 shows that $\gamma(0)=1.5$ and higher-lying γ trajectories do not appear to have α trajectory analogies, that the $\gamma(0)=0.89$ trajectory is the analog of the leading (first) α trajectory, and that the lower-lying γ trajectories are likely to be the analogs of lower-lying α trajectories. Also shown in Figs. 3(a) and 4 is one resonance of this Yukawa potential indicated by the single arrow.

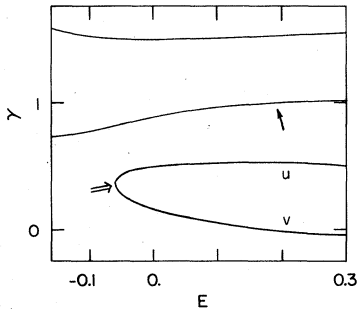

FIG. 4. An expanded view of the γ trajectories of the Yukawa potential $V(r)=-ge^{-r}/r$ with $g=8$ [see also Figs. 3(a) and 5]. Note that $l=1$, $E=0.19$ resonance on the second γ trajectory (single arrow), and the collision of the lower two (u and v) γ trajectories at $\gamma=0.37$, $E=-0.06$ (double arrow). The u and v trajectories are shown in the complex l plane in Fig. 5 for energies near their collision. All γ trajectories move smoothly through threshold $E=0$ (see text).

Beginning with the top trajectory in Fig. 3(a) and Fig. 4, the $\gamma(0)=1.5$ trajectory, we see that it starts at $l=1.5$ in Fig. 1(a) and thus is not associated with a shoulder of the phase shift δ. As the energy increases for $E>0$ this $\gamma(E)$ rises a little before settling back to 1.5 as E becomes large and δ goes to zero. The behavior of this $\gamma(E)$ near threshold (Fig. 4) is unusual relative to the threshold behavior of Regge trajectories and other γ trajectories in that it turns back up for $E<0$; more typical threshold behavior, at least for the lower-lying γ and α trajectories, is that displayed by the $\gamma(0)=0.89$ trajectory which does not turn back up for $E<0$. We have investigated the smoothness of the $\gamma(0)=1.5$ γ trajectory through threshold down to energies $|E|\geq 0.01$ and find that the trajectory passes through $E=0$ perfectly smoothly within these numerical limitations.

There do not appear to be any resonances or bound states associated with this $\gamma(0)=1.5$ trajectory so that it is not a particularly interesting trajectory; this is also true of all the higher-lying γ trajectories for this strength potential. These higher-lying γ trajectories start at $E=0$ at the half integers $\frac{5}{2}, \frac{7}{2}, \frac{9}{2}, \ldots$, and after rising a little fall back to the same half-integer from which they started as $E\to+\infty$; they have the same general character as the $\gamma(0)=1.5$ trajectory.

Turning now to the second [$\gamma(0)=0.89$] trajectory in Figs. 3(a) and 4, we see from Fig. 1(a) that this trajectory is associated with a shoulder of δ. Indeed, this γ trajectory "causes" the $l=1$ resonance at $E=0.19$ by passing through $l=1$ at $E=0.19$; recall that γ is real. This γ trajectory is the analog of the leading α trajectory for this potential.[2] The leading α trajectory also causes this $l=1$ resonance, but α "misses" (i.e., does not pass through) $l=1$ because α is complex for $E>0$. This example is a numerical illustration of the related, but different, ways the γ and α trajectories cause resonances: γ passes through the resonance angular momentum, while α passes near the resonance angular momentum; this phenomenon, central to the γ trajectory, is discussed in detail in TH.

Since this $\gamma(0)=0.89$ trajectory is the analog of the leading α trajectory for this potential, since both these trajectories cause the $l=1$, $E=0.19$ resonance, and since the $l=0$, $E\simeq-9$ bound state is on this leading α trajectory, it is reasonable to assume that this $\gamma(0)=0.89$ trajectory also causes the $l=0$, $E\simeq-9$ bound state. Unfortunately, this bound state lies too low to be accessible to our numerical method of computing

$\delta(E,l)$ (see Appendix A) and so we cannot explore this question. However, in the next section an explicit illustration of the connection of γ trajectories and bound states is given.

We have examined this $\gamma(0)=0.89$ trajectory in the neighborhood of threshold to the limits of the accuracy of the computational method for $\delta(E,l)$. We can approach $E=0$ with energies as close as $E\leq -0.0005$ and $E\geq 0.0005$, and an accuracy in the angular momentum l (and thus γ) of five to six significant figures. To this accuracy we find $\gamma(E)$ perfectly smooth across $E=0$; this result is consistent with the theory given in TH.

A last observation before leaving this γ trajectory is that inspection of Fig. 1(a) shows that as $E\to+\infty$, $\gamma(E)\to 0.5$ since $\delta\to 0$ in this limit.

The last two γ trajectories shown in Figs. 3(a) and 4 are those starting at $\gamma(0)=0.5$ and 0.17. (These trajectories are labeled also u and v, respectively.) As can be seen in Fig. 1(a) the lower of these trajectories is associated at $E=0$ with a shoulder of δ, while the upper trajectory is associated with a plateau. While these two trajectories appear to form a loop in Figs. 3(a) and 4, this is not the case; what happens is that the u and v trajectories "collide" at the point indicated in the figures by the double arrow ($\gamma=0.37$, $E=-0.06$), and "bounce off" each other into the complex l plane as the energy is lowered further than -0.06. This collision of u and v is shown in Fig. 5. The arrows on the u and v γ trajectories in this figure indicate the motion of the trajectories as the energy is increased; the trajectories shown are for energies starting at $E=-0.09$ and increasing to $E=0.00$. In calculating the trajectories u and v in Fig. 5 using Eq. (4), the energy is given a small imaginary piece (approximately 0.0005) which causes the trajectories to "miss" or "bounce off" each other as shown. In summary, the lower two γ trajectories (u and v) shown in Figs. 3(a) and 4 collide at $\gamma=0.37$, $E=-0.06$ (see double arrow) and move off into the complex l plane as shown in Fig. 5.

There is an $l=0$, $E=-0.11$ bound state of this Yukawa potential. Presumably this bound state is associated with one or both of the trajectories u and v although the mechanism is not as clear as that when trajectories do not collide and become complex (see next section). There are no other bound states or resonances associated with the u and v γ trajectories.

Inspection of Fig. 1(a) shows that the u γ trajectory goes to -0.5 as $E\to+\infty$, while the v γ trajectory goes (presumably) to -1.5 in the same limit (we do not calculate δ for $l<-0.5$).

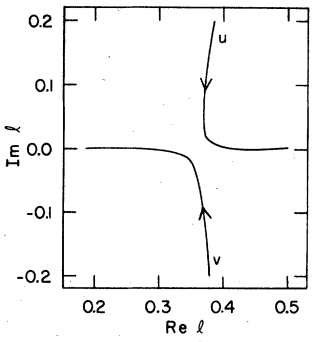

FIG. 5. The complex l plane. The solid curves are the paths of $\gamma(E)$ for the two lowest γ trajectories, u and v, of the Yukawa potential $V(r)=-ge^{-r}/r$ with $g=8$ [see Figs. 3(a) and 4 for other views of u and v]. The arrows indicate the direction of motion of the $\gamma(E)$ as the energy increases; the figure is for energy increasing from $E=-0.09$ to $E=0.00$. The trajectories collide at approximately $\gamma=0.37$, $E=-0.06$. The distance of closest approach is controlled by the imaginary part of E which is approximately 0.0005.

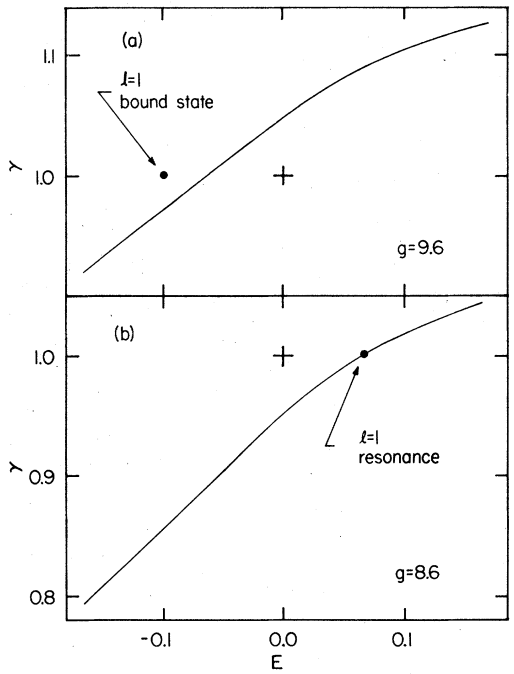

FIG. 6. γ trajectories in the region of $\gamma=1$ and threshold $E=0$ for the Yukawa potentials $V(r)=-ge^{-r}/r$ with $g=9.6$ (a) and 8.6 (b). (a) For $g=9.6$. The γ trajectory causes the bound state at $l=1$, $E=-0.1$ by passing near, but not through, the state angular momentum at the state energy (unlike the Regge trajectory α). (b) For $g=8.6$. The γ trajectory causes the $l=1$, $E=0.065$ resonance by passing through the resonance angular momentum at the resonance energy (unlike α). (a) and (b) The resonance for $g=8.6$ becomes the bound state as the potential strength is increased to $g=9.6$; the γ trajectory "follows" the state as g is increased.

B. Yukawa potentials: g=8.6, 9.6; bound states, resonances

In Figs. 6(a) and 6(b) is shown one γ trajectory in the neighborhood of $l=1$ and threshold $E=0$ for the two attractive Yukawa potential of strengths $g=9.6$ and 8.6, respectively. In Fig. 6(b) is indicated an $l=1$, $E=0.065$ resonance of the strength 8.6 potential. As the potential strength is increased from 8.6 to 9.6 the resonance at $l=1$, $E=0.065$ becomes the bound state at $l=1$, $E=-0.1$ as indicated in Fig. 6(a). In addition to the resonance moving below threshold and becoming a bound state as the potential strength is increased, inspection of Figs. 6(a) and 6(b) shows that the γ trajectory has also moved. In Fig. 6(b) the γ trajectory "causes" the $l=1$, $E=0.065$ resonance by passing through $l=1$ at the resonance energy. As mentioned earlier, this behavior is in contrast to that of the α trajectory which passes close to, but not through, $l=1$ at the resonance energy because α is complex for $E>0$. For the stronger potential ($g=9.6$) shown in Fig. 6(a), however, we see that the γ trajectory has moved upward as the potential strength has increased from 8.6 to 9.6, and that $\gamma(E)$ now causes, instead of the resonance, a bound state at $l=1$, $E=-0.1$. Unlike the α trajectory however, the γ trajectory "misses" the bound state by passing a little below it at the bound-state energy. In other words, the α trajectory has the bound-state l value at the bound-state energy, while the γ trajectory is below the bound-state l value at the bound-state energy, or alternately, has the bound-state l value at an energy above the bound-state energy.

These bound-state/resonance behaviors of the γ and α trajectories, illustrated in Figs. 6(a) and 6(b), are numerical examples of the contrasting means by which γ and α trajectories cause bound states and resonances: the γ trajectory passes through the resonance angular momentum at the resonance energy, while the α trajectory misses the resonance angular momentum at the resonance energy because it is complex. Below threshold, in the bound-state region, the reverse is true: Now the α trajectory passes through the bound-state angular momentum at the bound-state energy, while the γ trajectory misses the bound-state angular momentum at the bound-state energy in spite of being real. One could say that the γ trajectory causes resonances very much like the α trajectory causes bound states (by passing through the state), and vice versa, that the γ trajectory causes bound states very much like the α trajectory causes resonances (by passing near the state). In this sense the γ and α trajectories are complements of one another. (See TH for additional discussion.)

Finally, it can be noted, by comparing the γ trajectories in Figs. 6(a) and 6(b), that the γ trajectory rises as the potential strength is increased. In effect, the γ trajectory "chases" or is "dragged along by" the resonance/bound state so that it must rise as the potential strength is increased. This rising with potential strength is a general phenomenon which we see again in following sections.

C. Yukawa potential: g=10

In Fig. 3(b) is shown the low-lying γ trajectories of the attractive Yukawa potential of strength 10. These trajectories differ subtly from those of the strength 8 Yukawa potential shown Figs. 3(a), 4, and 5 and discussed previously. Comparing Figs. 3(a) and 3(b) one sees that $\gamma(0)=1.5$ for the highest trajectory shown for both $g=8$ and 10, that $\gamma(0)$ increases from 0.89 to 1.09 for the second trajectory as g increases from 8 to 10, and that for the bottom two trajectories the threshold value of the upper one is $\gamma(0)=0.5$ for both $g=8$ and 10, while the threshold value of the lower one increases from 0.17 to 0.36 as g increases from 8 to 10; thus, some of the $\gamma(0)$ values increase as g increases from 8 to 10, while others remained unchanged. This phenomenon is easily understood by inspecting Figs. 1(a) and 1(b). As the potential strength is increased from 8 to 10 the shoulders in Fig. 1(a) move to the right until they reach the position in Fig. 1(b). $\gamma(0)$ values which are half-integer come from the plateaus of $\delta(E,l)$; if the potential strength is increased only a modest amount, $\gamma(0)$ is still determined by the same plateau, and so is unchanged. In Figs. 1(a) and 1(b) this is seen to be true for the $\gamma(0)=0.5$ and 1.5 trajectories for both $g=8$ and 10. On the other hand, the other $\gamma(0)$ values come from the shoulders of $\delta(E,l)$; since these shoulders move as g increases, these $\gamma(0)$ move also. This explains the $\gamma(0)$ structure of Figs. 3(a) and 3(b).

A second observation about the $g=10$ γ trajectories is that the $\gamma(0)=0.89$ trajectory which causes the $l=1$, $E=0.19$ resonance for $g=8$ [Figs. 3(a) and 4] has moved upward to become the $\gamma(0)=1.09$ trajectory for $g=10$ [Fig. 3(b)]. This trajectory no longer causes a resonance, but instead now causes a bound state at $l=1$, $E\simeq-0.5$. This situation is entirely parallel to the discussion of the previous section of the $g=8.6$ and 9.6 Yukawa potentials where increasing the potential strength turns a resonance into a bound state.

Aside from the above remarks the $g=10$ γ trajectories are similar to the $g=8$ trajectories in all respects. Corresponding trajectories for the two potentials have the same high-energy limits,

e.g., and other properties are similar, including the collision of the two lowest trajectories below threshold (see double arrow).

D. Yukawa potential: $g=17$

The attractive Yukawa potential with strength $g=17$ has three $l=0$ and one $l=1$ bound states and several resonances. The low-lying γ trajectories for this potential are shown in Fig. 3(c), and one notes their similarities to the strength 8 and 10 γ trajectories. One should not conclude, however, e.g., that the $\gamma(0)=0.95$, $g=17$ trajectory that causes the $l=1$, $E=0.07$ resonance (see arrow) is the same trajectory as the $\gamma(0)=0.89$, $g=8$ trajectory that causes the $l=1$, $E=0.19$ resonance for that potential. These two trajectories, while similar in effect and in appearance, are solutions of Eq. (4) with different values of the integer n and so, e.g., have different high-energy limits. These and other differences between the $g=8$, 10 γ trajectories and the $g=17$ γ trajectories are due to fact that $\delta(E,l)$ for $g=17$ (not shown) has shifted to higher-l values relative to the δ's for $g=8$ and 10 shown in Fig. 1. Nevertheless, in spite of differences of detail, changing the strength of the Yukawa potential does not change the basic character of the γ trajectories; this fact is also true of the α trajectories.[2]

Starting from the top of Fig. 3(c) we see that the $\gamma(0)=1.65$ trajectory causes an $l=2$ resonance at $E=1.0$ (see arrow). This γ trajectory corresponds to the leading α trajectory which causes the same resonance and is associated also with two low-lying bound states (one $l=1$ and one $l=0$).[2]

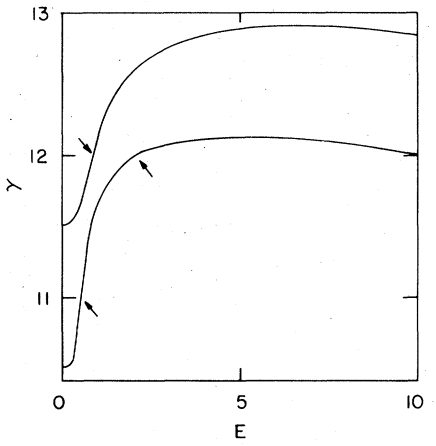

FIG. 7. Two γ trajectories of the exponential potential $V(r)=-43\exp(-r/2.5)$. The upper trajectory causes an $l=12$ resonance (see arrow) and passes through the half-integer $\frac{25}{2}$, while the lower trajectory causes $l=11$ and $l=12$ resonances (see arrows) and passes through the half-integer $\frac{23}{2}$.

The next γ trajectory shown, $\gamma(0)=1.5$, does not cause resonances. The third γ trajectory shown, $\gamma(0)=0.95$, causes an $l=1$ resonances at $E=0.07$ (see arrow). The bottom two γ trajectories shown collide (see double arrow) as in the $g=8$ and 10 cases; the threshold intercepts are $\gamma(0)=0.5$ and 0.20.

The high-energy limits of these $g=17$ γ trajectories are, respectively (starting with the top trajectory shown): $\frac{3}{2}$, $\frac{1}{2}$, $-\frac{1}{2}$, $-\frac{3}{2}$, and $-\frac{5}{2}$. These limits are lower than those of the $g=8$ γ trajectories, and comparison of Figs. 3(a) and 3(c) shows that the $g=17$ trajectories fall more rapidly with increasing energy than do the $g=8$ trajectories, if trajectories with similar $\gamma(0)$ values are compared. For example, if the $g=8$ and $g=17$ trajectories which cause $l=1$ resonances are compared, it is seen that the $g=17$ trajectory falls more rapidly with increasing energy.

E. Exponential potential

In Fig. 7 is shown two high-lying γ trajectories of the exponential potential $V=-43\exp(-r/2.5)$. This is a powerful, long-range potential which has many bound states and resonances. Although the general character of γ trajectories has already been illustrated using various strength Yukawa potentials, there are two properties of γ trajectories most easily shown using a strong exponential potential. First, both of the γ trajectories shown pass through half-integer angular momentum values: the higher trajectory passes through $\gamma=12.5$, while the lower trajectory passes through 11.5. This numerical example of γ trajectories going through half-integer values is an illustration of the special limiting process described in Sec. IIA. Second, the lower-lying γ trajectory in Fig. 7 causes two resonances; these states are at $l=11$, $E=0.56$ and $l=12$, $E=2.25$ (see arrows). The upper γ trajectory in Fig. 7 causes one resonance at $l=12$, $E=0.90$, and almost causes a second resonance with $l=13$. In principle, there is no reason why a single γ trajectory cannot cause a series of resonant states. Such a γ trajectory, of course, would at the same time pass through a series of half-integer angular momentum values.

IV. CONCLUSIONS

The main features of γ trajectories which are illustrated numerically in Sec. III, using various attractive Yukawa and exponential potentials are (1) γ trajectories are real for positive energies and for certain negative energies. (2) γ trajectories causes resonances and bound states much as do α (Regge) trajectories with the differences

that γ "passes through" resonances while α does not, and α "passes through" bound states while γ does not. (3) γ trajectories move through threshold smoothly. (4) some γ trajectories have the value of a half-integer at threshold, while other γ trajectories do not. (5) γ trajectories can collide below threshold and become complex. (6) γ trajectories can cause one or more resonances, and can pass through half-integer values of angular momentum. (7) As the energy becomes positive infinite the γ trajectories tend to half-integers.

Since the γ trajectory is real both above threshold and for certain regions below threshold, while the α trajectory is complex above and real below threshold, it might be concluded that the γ trajectory is "simpler" than the α trajectory. Indeed, above threshold the γ trajectory does appear to be more economical than the α trajectory, since γ causes resonances by passing directly through the resonance angular momentum. However, below threshold it is the α trajectory which is the more economical, since there α passes through the bound-state angular momentum at the bound-state energy. Thus, the γ and α trajectories appear to be complements of one another; they appear to have exchanged above-threshold and below-threshold behaviors.

As shown in TH, the γ trajectory can be used to analyze, e.g., pion-nucleon scattering data in the direct channel. Quite simple models of $\gamma(E)$ give excellent fits to the experimental pion-nucleon partial-wave amplitudes. However, it appears likely that the main interest of the γ trajectory is that it demonstrates that there exist other useful angular momentum trajectories besides the Regge trajectory α.

ACKNOWLEDGMENTS

We are indebted to our associates J. A. Cochran, H. B. Crawley, R. R. Hansen, J. P. Jarrett, R. L. Morrison, and B.-L. Young for support and helpful conversations. In particular, R. R. Hansen and R. L. Morrison provided invaluable assistance with the programs used to calculate the scattering phase shift, and J. A Cochran supplied helpful information on the numerical computation of Bessel functions. This work was supported by the U.S. Department of Energy, under Contract No. 7405-eng-82, Office of Energy Research, Division of High Energy Physics and Nuclear Physics.

APPENDIX A: PHASE SHIFT

The phase-function method is used to calculate the elastic scattering phase shift $\delta(E,l)$ in both the bound-state ($E<0$) and resonance ($E>0$) regions.[7] For $E>0$ the phase-function differential equation for $\gamma_l(r)$, the total phase function, is used. This differential equation is integrated by the standard Runge-Kutta fourth-order technique. In order to extract the phase shift $\delta(E,l)$ from the phase function $\gamma_l(r)$, the Ricatti-Bessel functions of complex argument and complex order are calculated using a program for Bessel functions based upon an asymptotic approximation.[8] The reason the $\gamma_l(r)$ phase-function differential equation is used instead of the $\delta_l(r)$ phase-function differential equation is because integrating the $\delta_l(r)$ equation requires the evaluation of the Ricatti-Bessel functions many times for each step of the integration, and this is much too slow a procedure. Each computation of $\delta(E,l)$ for given E,l requires about eight seconds on a PDP11 using the $\gamma_l(r)$ technique.

For $E<0$ the phase-function differential equation for $\tan\gamma_l(r)$ is used. Again this equation was chosen over the corresponding $\delta_l(r)$ equation for reasons of computational speed. Since the validity of the $\tan\gamma_l(r)$ differential equation had not been established previously for the $E<0$ region, a study of the $\tan\gamma_l(r)$ equation was performed; the result is that the $\tan\gamma_l(r)$ method is valid for $E<0$.[9] Again, $\delta(E,l)$ is extracted from $\tan\gamma_l(r)$. An important limitation of the phase-function technique for the calculation of $\delta(E,l)$ below threshold is that the energies accessable are confined to $\kappa<1/2r_0$, where κ is related to the energy by $E=-\kappa^2$ and where r_0 is the range of the potential.[7,9]

APPENDIX B: REALITY OF γ

In Sec. II C a proof that $\gamma(E)$ is real for $E>0$ was presented; that proof is based upon the properties of the phase shift $\delta(E,l)$. Another proof that $\gamma(E)$ is real above threshold follows from the radial Schrödinger equation and the properties of the radial wave function for angular momentum $l=\gamma(E)$. This proof, which is given here, is the analog of the proof that the Regge trajectory $\alpha(E)$ is real below threshold (see, e.g., Ref. 4, pages 106, 107).

First, writing the radial Schrödinger equation as (prime means d/dr)

$$u''+[k^2-V(r)-l(l+1)/r^2]u=0\,,$$

one obtains

$$(u^*u'-uu^{*\prime})\Big|_0^\infty-2il_I(2l_R+1)\int_0^\infty dr\,|u|^2/r^2=0\,, \tag{B1}$$

where the angular momentum is written $l=l_R+il_I$. Second, to use (B1) we need to evaluate the terms in it at the angular momentum $l=\gamma(E)$. Using Eq.

(4), $\delta(E,\gamma)/\pi = \gamma - (n+\frac{1}{2})$, one can find the S matrix and Jost functions at $l=\gamma$; thus, for $r\to\infty$, one has

$$u \simeq C(e^{i\pi\gamma}e^{ikr} + e^{-ikr}) \tag{B2}$$

where C is independent of r. Third, use of (B2) in (B1) yields

$$k(1-e^{-2\pi\gamma_I}) + \gamma_I(2\gamma_R+1)\frac{1}{|C|^2}\int_0^\infty dr|u|^2/r^2 = 0, \tag{B3}$$

where k is real and >0 and $\gamma=\gamma_R+i\gamma_I$. The integral is finite because of the oscillatory character of u, and because we require $\gamma_R > -\frac{1}{2}$ as in the discussion of the Regge trajectory $\alpha(E)$. Equation (B3) implies that the imaginary part of $\gamma(E)$ is zero; this completes the proof that γ is real above threshold. The fact that this proof is so parallel to the proof that α is real below threshold enhances the interpretation of γ and α as complements of one another.

---

[1]R. A. Leacock, preceding paper, Phys. Rev. D 20, 305 (1979), hereafter referred to as TH. See TH for discussion of the γ trajectory in a relativistic context, for γ-trajectory phenomenology, and for related references on the α trajectory.

[2]C. Lovelace and D. Masson, Nuovo Cimento 26, 472 (1962).

[3]By "half-integer" we mean, throughout this paper, "half-odd-integer," i.e., numbers such as $\frac{1}{2},\frac{3}{2},\cdots$.

[4]V. De Alfaro and T. Regge, *Potential Scattering* (North-Holland, Amsterdam, 1965), especially Chap. 5.

[5]See, e.g., J. R. Taylor, *Scattering Theory* (Wiley, New York, 1972).

[6]The reader is referred to the numerical study of Yukawa α (Regge) trajectories by Lovelace and Masson (Ref. 2) in order to compare the γ trajectories presented here with the corresponding α trajectories for the same potentials. Yukawa α trajectories are discussed, but not shown in the present work.

[7]F. Calogero, *Variable Phase Approach to Potential Scattering* (Academic, New York, 1967), especially Chap. 13.

[8]J. A. Cochran and E. J. Murphy, Bell Telephone Laboratories Technical Memorandum No. 72-1741-2, 1972 (unpublished). The program given in this memorandum calculates Bessel functions for which the absolute value of the order is greater than or equal to three; for smaller values of the order, recursion relations and expansions are used.

[9]J. M Clifton and R. A. Leacock (unpublished).